ResearchGate

See discussions, stats, and author profiles for this publication at: https://www.researchgate.net/publication/255796754

Atomic-resolution study of polarity reversal in GaSb grown on Si by scanning transmission electron microscopy

Article *in* Journal of Applied Physics · November 2012

DOI: 10.1063/1.4759160

CITATIONS
8

READS
46

6 authors, including:

Shahrzad Hosseini Vajargah
University of Waterloo
19 PUBLICATIONS **143** CITATIONS
SEE PROFILE

Shahram Tavakoli
McMaster University
21 PUBLICATIONS **88** CITATIONS
SEE PROFILE

Rafael Kleiman
McMaster University
109 PUBLICATIONS **2,402** CITATIONS
SEE PROFILE

John Stewart Preston
McMaster University
110 PUBLICATIONS **1,548** CITATIONS
SEE PROFILE

All content following this page was uploaded by Shahrzad Hosseini Vajargah on 17 November 2014.

The user has requested enhancement of the downloaded file. All in-text references underlined in blue are linked to publications on ResearchGate, letting you access and read them immediately.

Atomic-resolution study of polarity reversal in GaSb grown on Si by scanning transmission electron microscopy

S. Hosseini Vajargah, S. Y. Woo, S. Ghanad-Tavakoli, R. N. Kleiman, J. S. Preston, and G. A. Botton

Citation: Journal of Applied Physics **112**, 093101 (2012); doi: 10.1063/1.4759160
View online: http://dx.doi.org/10.1063/1.4759160
View Table of Contents: http://scitation.aip.org/content/aip/journal/jap/112/9?ver=pdfcov
Published by the AIP Publishing

AIP Publishing Re-register for Table of Content Alerts

Create a profile. Sign up today!

[This article is copyrighted as indicated in the article. Reuse of AIP content is subject to the terms at: http://scitation.aip.org/termsconditions. Downloaded to] IP: 193.62.126.232 On: Wed, 15 Jan 2014 22:01:27

Atomic-resolution study of polarity reversal in GaSb grown on Si by scanning transmission electron microscopy

S. Hosseini Vajargah,[1,2,3] S. Y. Woo,[1,2,3] S. Ghanad-Tavakoli,[4] R. N. Kleiman,[2,4,5] J. S. Preston,[2,4,5] and G. A. Botton[1,2,3]
[1]*Department of Materials Science and Engineering, McMaster University, Hamilton, Ontario L8S 4L7, Canada*
[2]*Brockhouse Institute for Material Research, McMaster University, Hamilton, Ontario L8S 4M1, Canada*
[3]*Canadian Centre for Electron Microscopy, McMaster University, Hamilton, Ontario L8S 4M1, Canada*
[4]*Centre for Emerging Device Technologies, McMaster University, Hamilton, Ontario L8S 4L7, Canada*
[5]*Department of Engineering Physics, McMaster University, Hamilton, Ontario L8S 4L7, Canada*

(Received 17 June 2012; accepted 19 September 2012; published online 1 November 2012)

The atomic-resolved reversal of the polarity across an antiphase boundary (APB) was observed in GaSb films grown on Si by high-angle annular dark-field scanning transmission electron microscopy (HAADF-STEM). The investigation of the interface structure at the origin of the APB reveals that coalescence of two domains with Ga-prelayer and Sb-prelayer causes the sublattice reversal. The local strain and lattice rotation distributions of the APB, attributed to the discordant bonding length at the APB with the surrounding GaSb lattice, were further studied using the geometric phase analysis technique. The crystallographic characteristics of the APBs and their interaction with other planar defects were observed with HAADF-STEM. The quantitative agreement between experimental and simulated images confirms the observed polarities in the acquired HAADF-STEM data. The self-annihilation mechanism of the APBs is addressed based on the rotation induced by anti-site bonds and APBs' faceting. © *2012 American Institute of Physics*. [http://dx.doi.org/10.1063/1.4759160]

I. INTRODUCTION

Heteroepitaxial III-V compound semiconductor layers grown on silicon have the potential to provide a range of new optoelectronic properties that make distinct applications beyond the Si-roadmap possible. Moreover, using Si as a substrate has the advantages of not only lower cost and less complexity but also large scale integration of compound semiconductors in the electronics industry. The lattice mismatch between Si and the heteroepitaxial layers as well as the formation of antiphase domains are two major obstacles that have to be overcome in order to grow device quality films. The III-Sb based compound family is one of the highly lattice-mismatched binary III-Vs with Si. However, the formation of an array of the interfacial misfit dislocations (IMFs) provides a complete relief of misfit strain between film and substrate.[1]

Antiphase domains, i.e., domains separated by antiphase boundaries (APBs), are an inherent hindrance to the growth of a polar film on a non-polar substrate. It is expected that the preferential initiation of the growth with one of the species in the epitaxial growth with molecular beam epitaxy (MBE) prevents the sublattice reversal during the nucleation of III-V compounds on Si. As a consequence, the intrinsic single atomic steps of the Si substrate surface[2] have been postulated as the main source for the APB formation. APBs are characterized by anti-site (wrong) bonds, i.e., cation-cation and anion-anion bonds. The APBs can be divided into three types: (a) boundaries with equal number of anti-site bonds of both elements (stoichiometric APBs), (b) boundaries with solely the wrong bonds of either III-III or V-V, and (c) a mixture of an unequal number of them (where the latter two types are non-stoichiometric APBs). The stoichiometric APBs occur on {110} and {211} planes; however, APBs on {100} and {111} planes are comprised exclusively of the same anti-site bonds (i.e., all III-III or V-V bonds) while APBs on {113} planes contain an unequal mixture of both type of wrong bonds (both III-III and V-V bonds).[2–5] Calculations of the formation energy of APBs from the simple wrong-bond counting method[6] to more sophisticated approaches based on first principles and density functional theory (DFT)[8,9] suggest that the {110} APBs have the lowest formation energy. Moreover, formation energy studies theoretically propose some models for self-annihilation of initially {110}-oriented boundaries based on occasional kinks[7] and faceting to other low formation energy planes such as {112} and {113}.[7,8] The faceting of APBs has been observed in GaP/Si and GaAs/Si and has been suggested as a possible mechanism of self-annihilation.[2,10–15] Molina *et al.* have also suggested that APBs do bend due to interaction with dislocations and consequently are annihilated.[16] It has experimentally been observed that a regular array of steps, induced by the slight misorientation of the substrate surface towards specific directions, promotes the APB's self-annihilation in GaAs on group IV substrates.[14,15,17–24] Furthermore, high temperature annealing of offcut substrates leads to the formation of the double-atomic height steps and APB suppression.[25–28]

The characterization of APBs is therefore not only important to understanding the origins of the defect formation but is also relevant since APBs are electrically active defects. In fact, APBs act as non-radiative recombination centers[10,29,30]

 © 2012 American Institute of Physics

[This article is copyrighted as indicated in the article. Reuse of AIP content is subject to the terms at: http://scitation.aip.org/termsconditions. Downloaded to] IP: 193.62.126.232 On: Wed, 15 Jan 2014 22:01:27

and as a result are the most deleterious planar defect[30] for many applications. APBs have been studied through a variety of transmission electron microscopy (TEM) techniques including convergent beam electron diffraction (CBED) developed by Taftø and Spence,[4,13,31–33] dark-field imaging with two opposite ±200 superlattice reflections,[2,11,34,35] and two-beam condition dark-field imaging using the 200-type superlattice reflections.[16,36] The APBs observed in these studies have been characterized using two distinct types of contrast: stacking fault-like fringes due to the inclination of the boundary with respect to the imaging surface and edge-on lines for APBs parallel to the electron beam.[2,16,33,35,37] These TEM techniques can be used for the investigation of the phase contrast produced by the rigid body translation of the wrong bonds.[4,38,39] Moreover, the interactions of the APBs with dislocations, grain boundaries,[3,33] and twins[33,40–43] have been detected using conventional TEM. However, the identification of the polarity reversal in specimens with constituent atoms of large difference in atomic scattering factor such as GaSb using the CBED technique is challenging. In addition, investigations of the atomic arrangement at the interface between the film and the substrate using high resolution transmission electron microscopy (HRTEM) are also challenging due to the strong dependency of images on specimen thickness and defocus conditions.[41,44] Therefore, misidentification of APBs with other planar defects, e.g., microtwins, can lead to imprecise conclusions on the effectiveness of the substrate type and growth conditions.[45]

Scanning transmission electron microscopes (STEMs) equipped with spherical aberration correctors have played a prominent role in pinpointing the atomic configuration of interfaces and defects.[1] The contrast mechanism exploited in the high-angle annular dark-field (HAADF) technique in STEM is strongly correlated with the atomic number of the scattering atoms.[46] It is also used for direct determination of local lattice polarity in the wurtzite structure.[47] Hence, HAADF can unambiguously elucidate the precise configuration of APBs and their origins. This technique is therefore able to reveal the influence of the substrate surface or nucleation condition on the structure of the APBs. When combined with a dedicated environment of the microscope with reduced levels of mechanical vibration, electromagnetic fields, and thermal fluctuations, HAADF-STEM enables the measurement of the atomic displacements at the defects sites via the geometric phase analysis (GPA) method.[1] Therefore, imaging of APBs using HAADF-STEM can reveal their atomic configuration and crystallographic nature, thus providing feedback on effective methods of suppressing the APBs. Additionally, the quality of the growth methods can be judged without misidentification of the defects[45] so that newer methods and approaches can be developed to assist in growing APB-free films.

In the present study, we report a detailed analysis of APB configurations in GaSb using HAADF-STEM and the possible causes of these defects. Using the GPA method, we have carried out quantitative measurements of the APB's strain distribution in order to eliminate any possible ambiguities regarding the structure of the APBs and we also determine the likely reasons for the faceting in APBs.

II. EXPERIMENTAL

A. MBE growth

GaSb epilayers were grown by SVT Associates MBE on a nominal (001) ± 0.5° Si substrate. Si wafers were chemically treated with 4% HF in DI water dipped for 1 min and rinsed with DI water for 30 s prior to use. Then the Si substrate was inserted immediately into the growth chamber and underwent degassing at 350 °C for 15 min and subsequently heat treated at 800 °C for 5 min to facilitate surface reconstruction. The epitaxial samples were prepared by depositing 5 nm of an AlSb buffer layer at a rate of 0.1 monolayer/s followed by a 500 nm GaSb film at 600 °C. A strained-layer superlattice (SLS) consisting of 25 alternating AlSb and GaSb epilayers of 10 nm thickness was grown to prevent the propagation of threading dislocations to the film surface. The SLS was finally covered with a 1 μm GaSb layer. The deposition rate of the GaSb and AlSb layers in the SLS was 1.0 μm/h and 0.6 μm/h, respectively. The GaSb capping layer was grown at the same rate as in the SLS.

B. TEM specimen preparation

The cross-sectional TEM specimens were polished mechanically using Allied High Tech MultiPrep™ System. The polished wedge specimens were then cleaned by a Technoorg Linda Gentle-mill with 300-800 eV Ar ions for approximately 60 min to remove the residue of polishing contamination. This method of sample preparation has previously produced very high quality specimens for aberration-corrected microscopy observations.

C. Image simulations

Image simulations were performed using the multislice simulation code developed by Kirkland.[48] This program can simulate the annular dark-field (ADF) images with input structural models, sample thickness and imaging parameters based on the experiments (C3 = 2 μm and C5 = 2 mm, the third and fifth order aberrations, respectively). These resulting simulated images are in qualitative agreement with the experimental images, although the contrast is higher in the simulations due to the non-zero size of the experimental illumination source. In order to model the source size to a first approximation, the simulated HAADF images are convolved by a Gaussian envelope function with a FWHM of 0.03 nm, thus reducing the resultant spatial coherence.

D. TEM characterizations

Phase contrast observations and CBED characterization to identify the APBs and perform polarity studies were performed on a Philips CM12 conventional TEM fitted with a LaB_6 filament operating at 120 keV. The ultrahigh-resolution Z-contrast HAADF images were obtained using a FEI Titan 80-300 "cubed" equipped with a high brightness field-emission gun, an electron monochromator, and CEOS spherical aberration (C_s) correctors of the probe and image forming lenses.

In order to analyze the strain of defects and interfaces, the HAADF-STEM images were processed with the GPA

[This article is copyrighted as indicated in the article. Reuse of AIP content is subject to the terms at: http://scitation.aip.org/termsconditions. Downloaded to] IP: 193.62.126.232 On: Wed, 15 Jan 2014 22:01:27

method using scripts written within the DIGITAL MICROGRAPH software package based on the work of Hÿtch *et al.*[49] and implemented commercially in HREM RESEARCH™ software. The GPA method is based on the concept that any lattice distortion or displacement and the corresponding strain cause a phase shift in the periodic pattern in the lattice image. Consequently, by measuring the phase changes of the lattice image, the corresponding strain and rotation can be calculated with respect to a chosen reference area in the image.

III. RESULTS

Fig. 1(a) shows the two-beam condition dark-field (DF) image obtained with the superlattice reflection g = 002. As the strain field of the SLS repels the dislocations and forces them to bend toward the substrate, the density of threading dislocations propagating to the film surface decreased beyond the SLS. The red arrows in Fig. 1(a) show the area featuring an APB in the GaSb film which has initiated from the interface with Si and propagated to the epilayer surface. The APB is invisible in the bright-field (BF) image with fundamental reflection g = −220 (Fig. 1(b)) since the displacement of the APB satisfies the g.R = 0 criterion. This verifies that the observed defect is likely an APB. The polarity studies with CBED also confirmed the polarity reversal across the APB.[50] As is seen in Fig. 1(a) the majority of the facets in the APB lie on or close to {110} planes and are perpendicular to the viewing direction. However, sections of the APB with stacking-fault like fringes indicate the inclination of the boundary with respect to the transmitting electron beam. Based on formation energy calculations[6–9] the {110}-oriented APBs have the lowest formation energy and hence are expected to be the most favored type of APBs in the zinc-blende structure.

In HAADF imaging, the bond polarity can be identified both in GaSb and AlSb. Fig. 2 displays the HAADF-STEM image of the interface between AlSb layer (right side) and GaSb layer (left side) in the SLS area of the heterostructure. The interface appears atomically sharp without any noticeable intermixing. There is a strong contrast between the atomic columns in the GaSb and AlSb regions. The polarity of GaSb bonds is resolved as Sb atoms appear brighter than Ga atoms according to their atomic numbers. However, the Al atoms appear as faint tails next to the Sb atoms due to the low Z number of Al. The HAADF-STEM simulations (Figs. 2(b) and 2(c)) obtained with imaging conditions similar to those of the experiments confirm the main features deduced from the experimental micrographs. The polarity of GaSb and AlSb bonds in the simulated images is consistent with the experimental image with the Sb atoms appearing brighter than the Ga atoms, while the Al atoms are not discernible in the AlSb film. The HAADF-STEM simulation results also indicate that the difference between the intensities of the Sb and Ga columns are not distinguishable in samples with thicknesses greater than 60 nm due to the strong column-to-column scattering. The Z-number dependence of the intensity in the HAADF-STEM images thus offers exquisite sensitivity to the atomic number in very thin samples.

We can put to use this sensitivity to the bond polarity in the identification of APBs in the SLS. Here, the presence of APBs in the AlSb region is more easily detected due to the changes in the intensity of the Al columns. Fig. 3(a) illustrates a polarity swap between the right and left regions of the micrograph within the APB region highlighted between the arrows. The region where the reversal of the bond directionality is visible in the image is much broader than the simple ball and stick model of a {110}-oriented APB (Fig. 3(b)) and extends to a width of 3.3 nm. The Al columns in AlSb are practically not detected in the HAADF image. However, in the APB region, the intensity of the nominal Al columns increases noticeably. The increase in the intensity of the Al columns in the middle of the boundary region indicates that a fraction of Al atoms within the column is replaced by Sb atoms and that a fraction of Sb atoms is replaced by Al atoms. The width of the APB region also indicates that the APB plane is not perfectly parallel to the electron beam. In order to further confirm these assumptions, an arbitrarily chosen {310}-oriented APB is simulated with the multislice approach in the GaSb (Fig. 3(c)) and AlSb (Fig. 3(d)) structures. The {310} plane is perpendicular to the (001) surface but inclined with respect to the {110} planes and thus the electron beam. In the simulated images Figs. 3(c) and 3(d), the atoms interchange their sites across the APB, both in the GaSb and AlSb layers. The gradual change in the intensity of the Al columns in the simulations (Fig. 3(d)) is consistent with the experimental image and can thus be explained solely with the presence of the APB without inter-diffusion

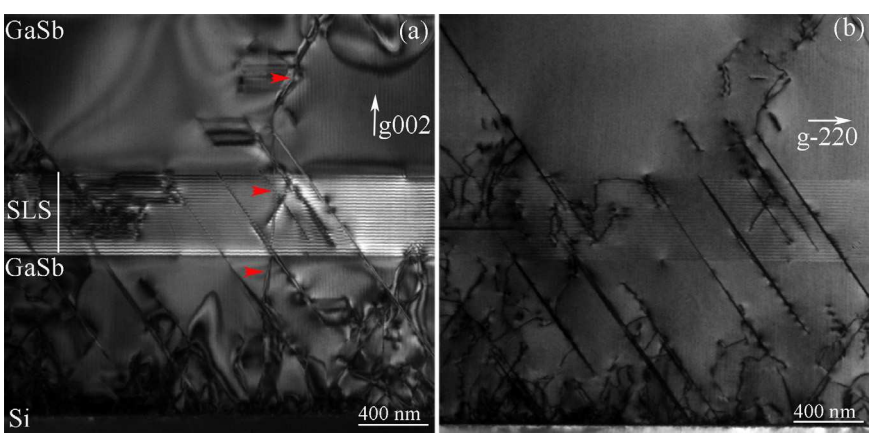

FIG. 1. TEM two-beam images of the area featuring APBs. (a) DF image with superlattice reflection g = 002, red arrows are highlighting the APB originating from interface and propagating to epilayer surface. (b) BF image with fundamental reflection g = −220.

[This article is copyrighted as indicated in the article. Reuse of AIP content is subject to the terms at: http://scitation.aip.org/termsconditions. Downloaded to] IP: 193.62.126.232 On: Wed, 15 Jan 2014 22:01:27

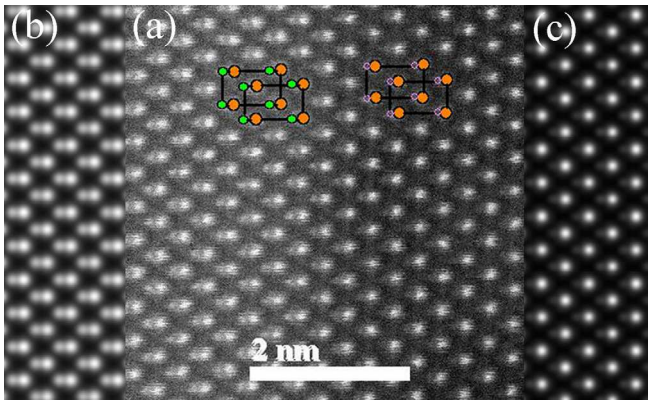

FIG. 2. (a) Experimental HAADF-STEM image of an atomically sharp interface of the AlSb and GaSb layer in the SLS. HAADF-STEM simulation of (b) GaSb and (c) AlSb in ⟨110⟩ projection for a sample thickness of 20 nm, and similar microscope parameters as in experiments.

of atoms within the APB. The consistency of the simulation with our experimental images also supports the assumption that the Sb atoms have replaced Al atoms through the thickness of the TEM foil and hence that the boundary is inclined with respect to the viewing direction. It is also inferred that the APB is lying on a higher index crystallographic plane which is inclined with respect to {110} planes but perpendicular to the (001) surface. The schematic atomic model of the simulated APB (Fig. 3(d)) is shown in Fig. 4(a). The model demonstrates an {310}-oriented APB that propagates vertically with respect to the interface but is inclined with respect to the viewing direction, i.e., the {110} planes. Fig. 4(b) displays the side view (perpendicular to the electron beam

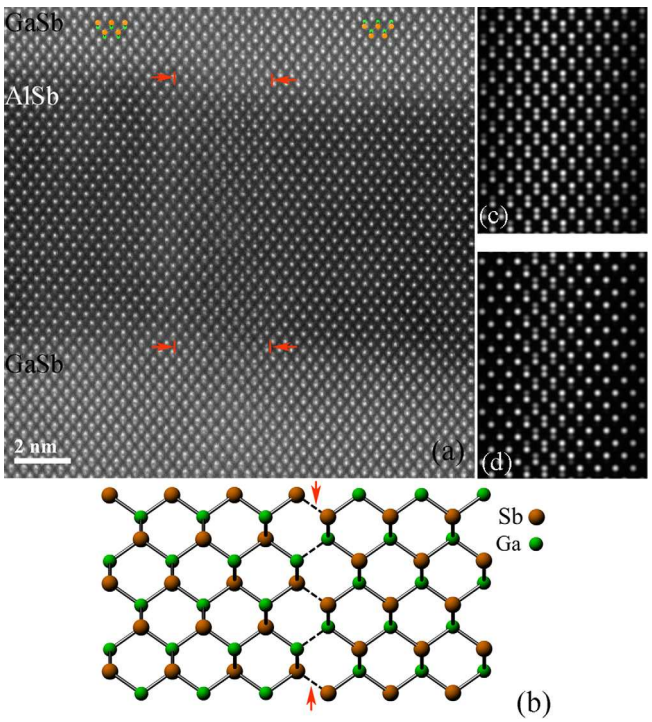

FIG. 3. (a) HAADF-STEM image of alternating GaSb and AlSb layers in the SLS, red arrows outline an APB crossing the SLS and (b) schematic of a {110}-oriented APB, the dashed line highlights the wrong bonds between same-type atoms. Multislice simulation of an arbitrarily chosen {310}-oriented APB in (c) AlSb and (d) GaSb.

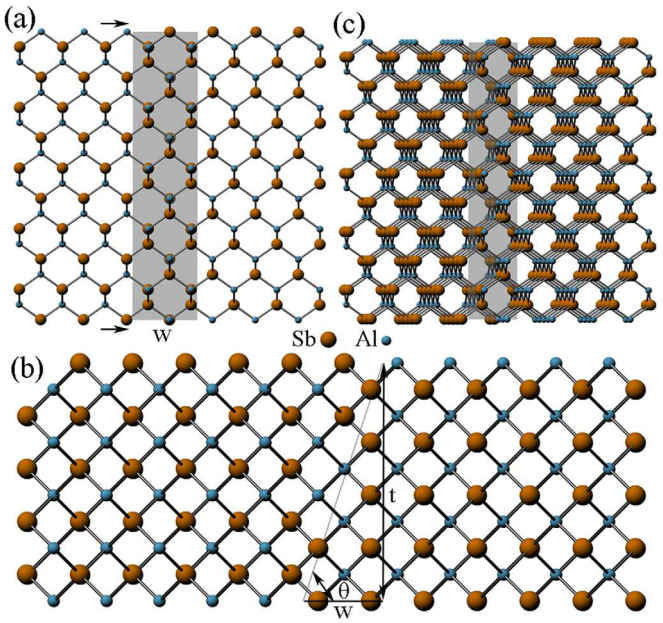

FIG. 4. (a) Schematic projection of an arbitrarily chosen {310}-oriented APB perpendicular to {001} and inclined to [110] view direction, the arrows show the top surface of the specimen, **w** is the width of the ABP in projection, (b) side view of the plane in (a) along [001] view direction, **t** is the thickness of sample in the region of the APB and θ is the angle between APB and the projection plane, and (c) partial or complete replacement of Al atoms with Sb atoms depending on the location of the intersection of the APB plane and Al columns.

direction) of the same model in which θ is the angle between the APB plane and the projection plane. The angle θ can be calculated using the thickness (t) of the sample and width (w) of the APB. The partial or complete replacement of the Al atoms with Sb atoms through the thickness of the specimen can be seen in Fig. 4(c). The number of Al atoms that are replaced by Sb depends on the location of the intersection of the APB plane and atomic column and hence the intensity of the atomic column changes accordingly.

In order to understand the origins of the formation of the APBs, we focus on the APBs at the interface between GaSb and Si. Fig. 5(a) displays an APB right at the interface between the Si substrate and the GaSb film which propagates into the film. In this case, the APB is a {110}-oriented boundary that originates vertically from the interface. The APB in Fig. 5(a) appears as a line rather than a band unlike the APB in Fig. 3(a), thus it lies parallel to the direction of the transmitting electron beam. From the change in contrast between the Ga and Sb columns, it is possible to identify the precise location of the APB and show that the boundary deviates from the initial vertical orientation at the interface to an average irrational plane. Large segments of the boundary have faceted to other crystallographic planes for lengths of few unit cells. However, segments lying on or close to {211} planes and the other {011} planes, leaning 45° from the interface normal, can be identified. The lower HAADF signal intensities apparent on the left and right sides of the HAADF image point out the presence of AlSb islands used as a buffer layer to promote a fully relaxed planar film of GaSb as pointed out in our previous work using energy dispersive X-ray spectrometry mapping.[1] The other planar

[This article is copyrighted as indicated in the article. Reuse of AIP content is subject to the terms at: http://scitation.aip.org/termsconditions. Downloaded to] IP: 193.62.126.232 On: Wed, 15 Jan 2014 22:01:27

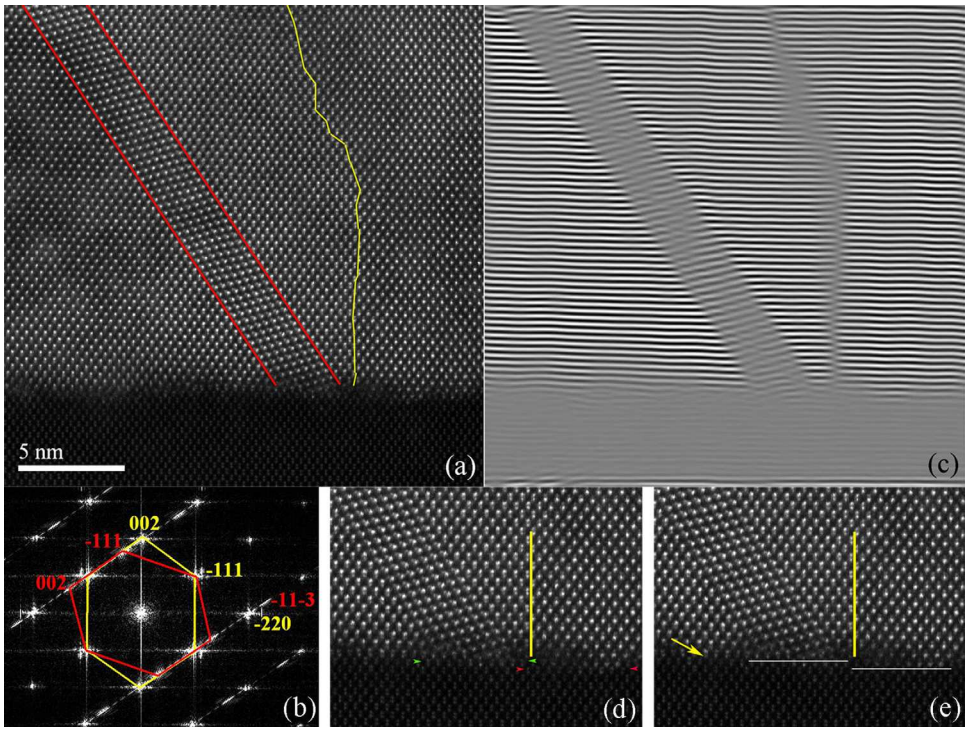

FIG. 5. (a) The HAADF-STEM image of GaSb-Si interface with an APB (outlined with yellow line), (b) Fourier transform of the image, red and yellow indices show the Bragg reflections of the twinned and epitaxial GaSb, (c) the Fourier filtered image of (a) using the (002) reflection. The 1/4 a ⟨001⟩ displacement along the growth direction is distinguishable at the APB, (d) the magnified image of interface at the APB in (a) with arrows displaying the last atomic plane of Si and (e) the white lines are drawn on the last atomic plane of Si on either side of the boundary to show the double atomic high step at surface. The arrow highlights a domain starting with Ga-prelayer.

defect highlighted with red lines is a first-order twin with {111} habit plane lying at an angle of 54.7° from the interface. Fig. 5(b) is the Fourier transform of the image in which the yellow and red indices belong to the epitaxial and twinned GaSb, respectively. As seen from the image, the microtwin gives rise to additional twin reflections in the form of streaks which are rotated with respect to the epitaxial GaSb. The displacement of the (001) atomic planes along the growth direction [001] can be observed by Fourier filtering using the (002) reflection. As seen in Fig. 5(c), the (002) atomic planes are displaced half of the (002) interatomic distance along growth direction which is equal to 1/4 a ⟨001⟩. The detailed view of the interface region where the APB intersects the substrate further highlights the last atomic plane of Si (Figs. 5(d) and 5(e)). In Fig. 5(d), the last atomic plane of the substrate is indicated by arrows on both sides of the APB. The white lines drawn on the last atomic plane of the Si substrate show a double atomic-high step at the interface (Fig. 5(e)). The arrow on the left side of Fig. 5(e) also highlights the first atomic monolayer of lower intensity than the right side of the APB which is assumed to be Ga-prelayer domain.

To avoid the possible misinterpretation of the intensities in an image of the interface due to the channeling effect of the electron beam, multislice simulations were carried out on the structure shown in Fig. 6(a). Fig. 6(a) is a ball and stick structural model of an APB resulting from the coalescence of a Ga-prelayer domain (left side) and a Sb-prelayer domain (right side) originating from mixed nucleation on the surface of a flat (001) Si substrate. Two dangling bonds of the surface-layer Si atoms are oriented perpendicular to the interface between Si and GaSb which is the more energetically favorable configuration when a double step exists on a Si surface.[51] On the other hand, in this configuration of the interface layer, the left and right sides are comprised of Ga-Si and Sb-Si dumbbells, respectively. Since the mixed dumbbells adjacent to the interface are the closest species, we have to consider the possible channeling from the Sb/Ga column to the Si column and back to the Ga/Sb column and the effect of the mixed pair on interpretation of the image intensity of the individual columns. The multislice HAADF-STEM simulations of the model with a sample thickness of 20 nm (Fig. 6(b)) indicate that the intensity of the Ga column in the Ga-Si pair and the intensity of the Sb column in the Sb-Si pair are distinguishable. The intensity profiles of the left (Fig. 6(c)) and right (Fig. 6(d)) sides of the APB clearly demonstrate that the intensity of an Sb atom in an Sb-Si pair is approximately similar to the intensity of an Sb atom in a Ga-Sb dumbbell and furthermore that the Sb atom at the first monolayer is noticeably brighter than the Ga atom in the first monolayer. This observation implies that the intensity of HAADF-STEM images with a specimen thickness 20 nm and below can be interpreted reliably.

The Bragg reflections $g_1 = 002$ and $g_2 = -220$ in the Fourier transform of the image in Fig. 7(a) were analyzed using a Gaussian mask with the size of $1.09\,\text{nm}^{-1}$ in reciprocal space resulting in $1/1.09 = 0.91$ nm spatial resolution. From the resulting phase image (Fig. 7(a)), it is clear that the phase of the two adjacent domains shifted from 0 to π (or $-\pi$) due to the half inter-planar spacing displacement of the atoms across the APB. The π phase shift in Fig. 7(b) is consistent with the polarity reversal characteristic of the APBs. Figs. 7(b) and 7(c) display the in-plane strain fields ε_{xx} and ε_{yy}, respectively, derived from GPA. The strain maps in Figs. 7(c) and 7(d) show the smaller lattice constant of the Si substrate (negative apparent strain) defined with respect to the reference lattice of the GaSb film. The visibility of the APB is more pronounced in the ε_{yy} map (Fig. 7(c)) as a result

[This article is copyrighted as indicated in the article. Reuse of AIP content is subject to the terms at: http://scitation.aip.org/termsconditions. Downloaded to] IP: 193.62.126.232 On: Wed, 15 Jan 2014 22:01:27

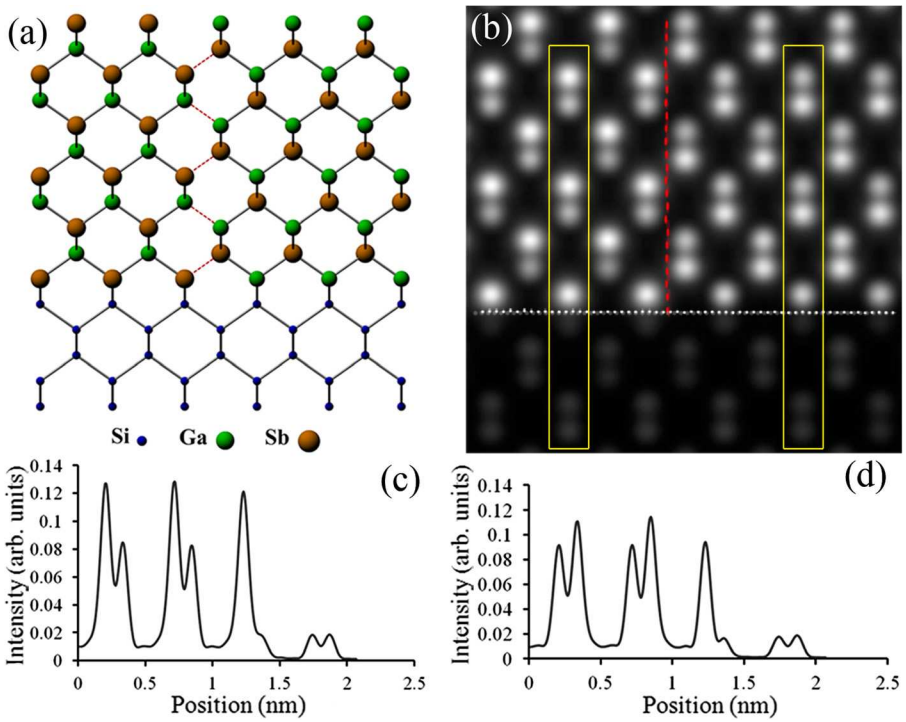

FIG. 6. (a) The ball and stick model of a {110}-oriented APB marked by red dashed line and (b) Multislice HAADF-STEM simulation of the superlattice in (a) for a specimen thickness 20 nm. Intensity profile of (c) left side and of (d) right side of the APB boxed in yellow. The GaSb and Si interface is highlighted by white dotted line.

of the larger strain component along y (growth direction) than along x (parallel to interface). It is also apparent that the strain is larger in the curved segment of the APB than the edge-on segment. The strain field of the twin adjacent to the APB is apparent as well. The measurement of the local apparent strain in the ε_{xx} map indicates that there is a 4% strain between Si and the twinned GaSb. This strain corresponds to the mismatch between {113} planes of the twinned GaSb and {022} planes of the Si substrate which were included inside the mask used for calculating of the phase images. In Fig. 7(d), the in-plane rotation matrix of Fig. 7(a) is shown in which the positive and the negative angles correspond to counter-clockwise and clockwise rotations of the lattice, respectively.

To study the strain distribution of the interfacial misfit dislocations, the (-111) and (1-11) Bragg reflections were evaluated with the GPA method (Fig. 8(a)). The positive apparent strain of GaSb film is indicative of its larger lattice constant with respect to the Si substrate reference lattice. The black arrows on the image show the core of the misfit dislocations with spacing smaller than the 90° Lomer dislocations in the GaSb/Si heterostructure.[1] The rotation of the twinned GaSb lattice with respect to the epitaxial GaSb and the Si substrate can also be seen in Fig. 8(b).

Based on the visibility of the APB in HAADF images and the reversal of the polarity of dumbbells, we can now demonstrate how APBs interact with other defects in thin films. Figs. 9(a) and 9(b) illustrate the interactions of the APB, highlighted with a yellow line, with a nano-twin. In

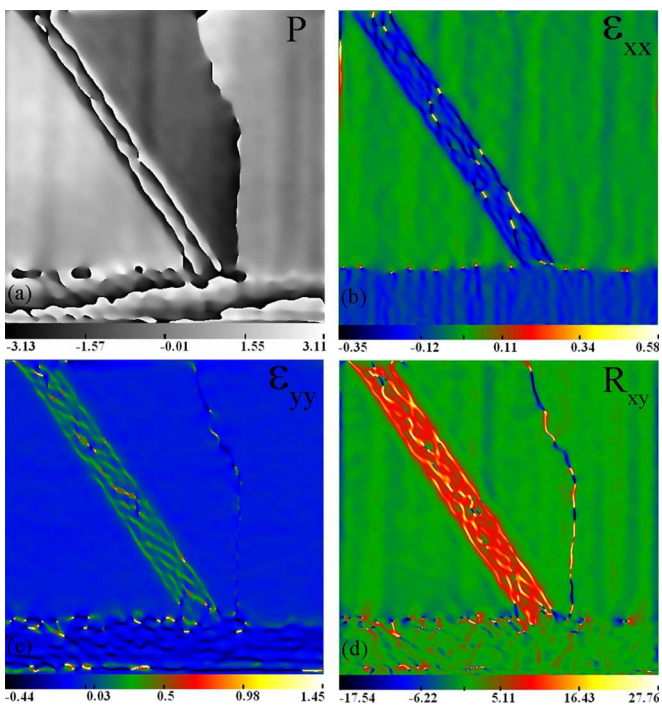

FIG. 7. (a) Phase image of the (002) Bragg reflection. The strain map (b) parallel (ε_{xx}) with and (c) perpendicular (ε_{yy}) to the interface, and (d) the rotation matrix (R_{xy}). GaSb lattice is used as the reference lattice.

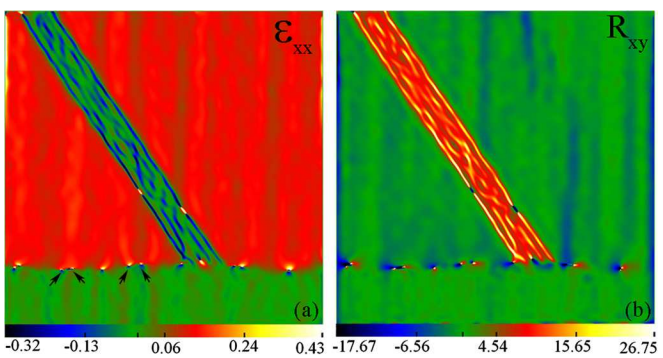

FIG. 8. (a) Strain map ε_{xx} along the interface and (b) Rotation map R_{xy}. Si lattice is used as the reference lattice.

[This article is copyrighted as indicated in the article. Reuse of AIP content is subject to the terms at: http://scitation.aip.org/termsconditions. Downloaded to] IP: 193.62.126.232 On: Wed, 15 Jan 2014 22:01:27

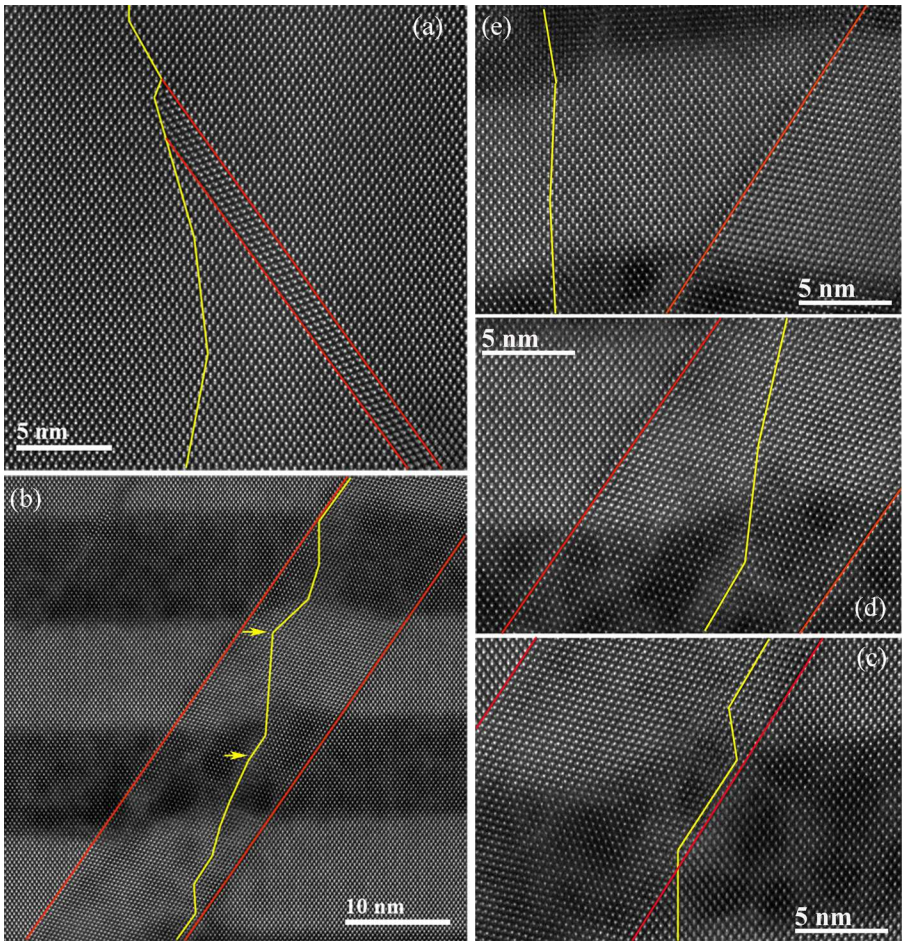

FIG. 9. APB and twin boundary intersections are outlined with yellow and red lines, respectively. (a) Twin blockage and APB propagation and (b) propagation of both APB and twin. The APB in (b) is shown in (c) entering into the twin region, (d) bent by the twin, and (e) exiting from the twin region. Section (d) is the magnified image of part of the APB highlighted with yellow arrows in (b), while sections (c) and (e) are magnified images of the sample shown in (b) from regions below and above, respectively.

Fig. 9(a), the APB prevents the propagation of the nano-twin (4 atomic planes wide) and thus terminates the twin. However, in Fig. 9(b), the APB (entering from the highlighted region in Fig. 9(c)) is bent by the twin (displayed in Fig. 9(d)), propagates some distance along the twin, and eventually exits from it (shown in Fig. 9(e)). The reversal of Ga-Sb dumbbell orientation across the APB path in Fig. 9(d) is visible. Because of the interaction between the twin and the APB, the position of the SLS interfaces changes (Fig. 9(b)) indicating that the growth rate is affected not only by the twin as reported in Ref. 44 but also by the APB.

IV. DISCUSSION

It is common for APBs to form on some low-index crystallographic planes such as {110}, {211}, and {111}. However, our observations using HAADF-STEM technique shows that APBs can lie on a variety of crystallographic planes such as some uncommon high index crystallographic planes (Fig. 3(a)). Large segments of {110}- and {211}-oriented APB planes in Fig. 5(a) display that the APBs preferably originate on stoichiometric planes and retain their stoichiometric characteristics by faceting accordingly due to energetics and interface neutrality considerations.[6–9] However, if there is any change in the intrinsically stoichiometric growth conditions of the MBE such that it deviates from stoichiometry, we can expect it will induce APBs of the non-stoichiometric type, such as {111} planes.

The domain with a Ga-prelayer in Fig. 5(d) unambiguously indicates that mixed domain nucleation has induced this APB. This phenomenon implies that the initiation of growth with Sb-prelayer soaking cannot guarantee that Sb will overlay on the Si substrate as the first atomic layer. Unlike GaAs/Si where As soaking can prevent mixed nucleation,[52] in GaSb growth the low sticking coefficient of Sb to Si can cause Ga-prelayer and Sb-prelayer domain formation.[50,53] The ball and stick model in Fig. 10 shows that in spite of the presence of the double atomic high step, the sequence of the Sb and Ga layers on the either side of the step will not change. However, on the left side of Fig. 10, we introduced an APB forming due to the coalescence of the domain starting with Sb as the first monolayer with the Ga-prelayer domain. In the model, the starting point of the Ga-prelayer domain does not coincide with the double step to reduce the complexity of the model.

We have also pointed out that a lattice rotation can be detected in APBs. This strain and lattice rotation caused by the APB in Figs. 5(c) and 5(d) can be attributed to the different bond length of the anti-phase bonds compared to the in-phase bonds. The higher strain in the curved segment of the APB may be due to the unequal number of wrong bonds forming the APB. The strain of the lattice due to the presence of an APB relaxes and causes the adjacent atomic bond to shrink or stretch in order to accommodate the strain from the wrong bonds and hence results in a rotation of the lattice. The ball and stick model in Fig. 11 illustrates the influence of the bond

[This article is copyrighted as indicated in the article. Reuse of AIP content is subject to the terms at: http://scitation.aip.org/termsconditions. Downloaded to] IP: 193.62.126.232 On: Wed, 15 Jan 2014 22:01:27

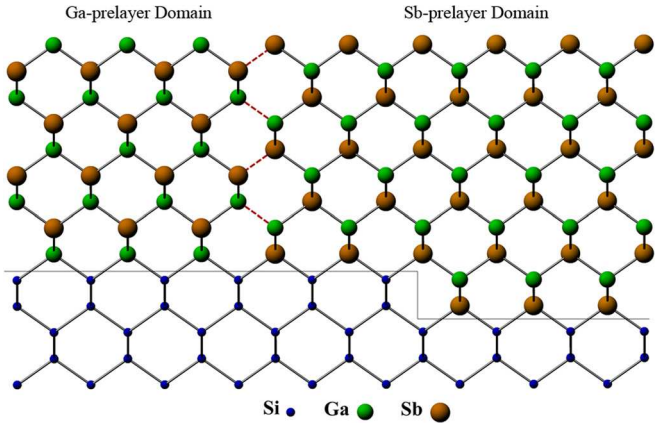

FIG. 10. Schematic model of a double atomic high step at the Si substrate showing the formation of an APB due to the coalescence of antiphase domains with Sb and Ga as their first monolayer. The dashed lines display the wrong bonds along the APB.

length on the rotation of the lattice due to the change in the wrong bonds lengths (Ga-Ga = 252 pm, Sb-Sb = 272 pm[4]) compared to the correct bond length (Ga-Sb = 262 pm). As pointed out by the arrows, the rotation direction of the bonds is induced by the change in the length of the Ga-Ga and Sb-Sb wrong bonds. When these clockwise and counter-clockwise rotations are unbalanced, there is a net rotation of the APB. The APB maintains its normal direction by counterbalancing the rotation; consequently the rotation direction is reversed for two consecutive sections of the APB (Fig. 5(d)). This change in the rotation direction may also be due to the local excess or deficit of Ga or Sb that make the small segments of {111}-oriented APBs favorable, similar to what Vanderbilt *et al.*[7] proposed based on their theoretical calculations.

Our observations reveal that all the APBs in GaSb were initiated normal to the substrate regardless of whether they propagate to the film surface or annihilate within the film.

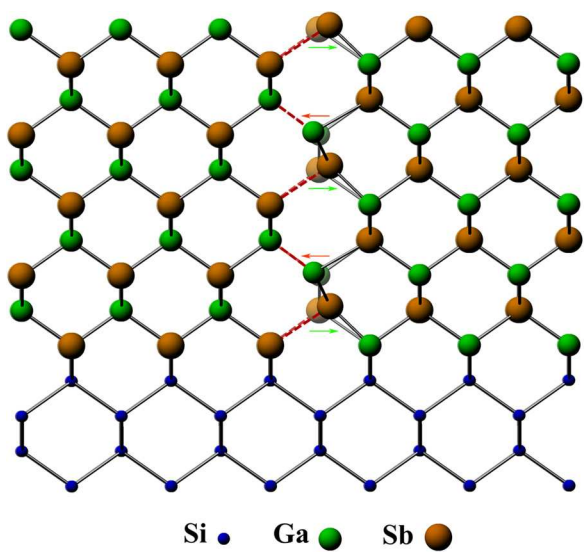

FIG. 11. Schematic of atomic bond distortion along the APB and the induced lattice rotations. The arrows show the rotation direction of the atomic bonds.

However, they often facet to other crystallographic planes and change their lateral positions. Sometimes two APBs with reversed kinking directions annihilate each other. It is believed that this faceting is due to local relaxation and lattice rotation to accommodate the change in bond length in addition to interfacial energy considerations. The proposed mechanism of the self-annihilation supports the theoretical work by Vanderbilt *et al.*[7] and suggests a possible reason for the kinking which was unclear in their work. The scarcity of the self-annihilated APBs on the flat substrate is the result of the larger step spacing of the substrate compared to offcut substrates. Because of this, the density of the self-annihilated APBs in the GaSb film grown on an offcut substrate is significantly higher than that on the flat substrate.[50] The number of closed-loop APBs may also increase by increasing the growth thickness.

It is clear from the strain map parallel to the interface (ε_{xx}) (Fig. 8(a)) that the lattice parameter in the GaSb film has relaxed to its bulk value with a mismatch of 12% with the Si substrate. The strain distribution of the dislocation cores shows that the GaSb lattice is under tension to accommodate the extra atomic half plane in the Si lattice. The dislocation core shown by the arrows belongs to two pairs of 60° dislocations on the distinct {111} planes that were not able to react to the 90° dislocations. The 60° dislocations are not as efficient as the 90° dislocations in accommodating the lattice mismatch. The rotation angle of the twin region corresponds to the first-order twining operation (the rotation of the {111} planes around the ⟨110⟩ foil normal). The annihilation of the twin boundary after the interaction with an APB has been attributed to the presence of a kinetic barrier[41] and a larger amount of disorder caused by the APB.[43]

V. CONCLUSION

We have demonstrated the atomic resolved configuration of APBs in GaSb grown on Si and their resultant polarity reversal. The direct detection of the presence of APBs from the HAADF-STEM micrographs avoids tedious polarity studies and allows very direct studies of the origin of the APBs and their interaction with other defects. The results presented show that the orientation of the APBs can be intuitively inferred from the Z-contrast images. The extracted phase images through GPA image processing illustrate the phase change across the APBs. The local measurements of the strain at the interface of domains with reversed polarity have revealed the strain induced by the incongruous bond length of the wrong bonds. Compensating the lattice rotation by lateral shifting and faceting plays an important role in the self-annihilation of the APBs. The prelayer soaking step plays a crucial role in the formation of the APBs. In order to reduce the formation of the APBs, precise control of the substrate offcut as well as the growth recipe should be implemented simultaneously. We have shown that interactions between APB and twin boundaries do not necessarily lead to annihilation of the twins, even if such annihilation has been observed in our work. Therefore, other factors dictating the resulting interaction between defects and APBs can still be present.

[This article is copyrighted as indicated in the article. Reuse of AIP content is subject to the terms at: http://scitation.aip.org/termsconditions. Downloaded to] IP: 193.62.126.232 On: Wed, 15 Jan 2014 22:01:27

ACKNOWLEDGMENTS

The authors gratefully acknowledge financial support of Ontario Centres of Excellence and ARISE Technologies. Electron Microscopy work was carried out at the Canadian Centre for Electron Microscopy (CCEM), a facility supported by NSERC and McMaster University.

[1]S. Hosseini Vajargah, M. Couillard, K. Cui, S. Ghanad Tavakoli, B. Robinson, R. N. Kleiman, J. S. Preston, and G. A. Botton, Appl. Phys. Lett. **98**, 082113 (2011).
[2]N.-H. Cho, B. C. De Cooman, C. B. Carter, R. Fletcher, and D. K. Wagner, Appl. Phys. Lett. **47**(8), 879–881 (1985).
[3]O. Ueda, T. Soga, T. Jimbo, and M. Umeno, Appl. Phys. Lett. **55**(5), 445–447 (1989).
[4]D. Cohen and C. B. Carter, J. Microsc. **208**(2), 84–99 (2002).
[5]D. B. Holt, J. Phys. Chem. Solids **30**, 1297–1308 (1969).
[6]P. M. Petroff, J. Vac. Sci. Technol. B **4**(4), 874–877 (1986).
[7]D. Vanderbilt and C. Lee, Phys. Rev. B **45**(19), 11192–11201 (1992).
[8]O. Rubel and S. D. Baranovskii, Int. J. Mol. Sci. **10**, 5104–5114 (2009).
[9]W. R. Lambrecht, C. Amador, and B. Segall, Phys. Rev. Lett. **68**(9), 1363–1366 (1992).
[10]S. N. G. Chu, S. Nakahara, S. J. Pearton, T. Boone, and S. M. Vernon, J. Appl. Phys. **64**(6), 2981–2989 (1988).
[11]I. Németh, B. Kunert, W. Stolza, and K. Volz, J. Cryst. Growth **310**, 1595–1601 (2008).
[12]K. Volz, A. Beyer, W. Witte, J. Ohlmann, I. Németh, B. Kunert, and W. Stolz, J. Cryst. Growth **315**, 37–47 (2011).
[13]A. Beyer, I. Németh, S. Liebich, J. Ohlmann, W. Stolz, and K. Volz, J. Appl. Phys. **109**, 083529 (2011).
[14]S. Koh, T. Kondo, T. Ishiwada, H. Sawada, H. Ichinose, I. Shoji, and R. Ito, Physica E **7**, 876–880 (2000).
[15]A. Georgakilas, J. Stoemenos, K. Tsagaraki, P. Komninou, N. Flevaris, P. Panayotatos, and A. Christou, J. Mater. Res. **8**(8), 1908–1921 (1993).
[16]S. I. Molina, G. Aragon, R. Garcia, Y. Gonzalez, L. Gonzalez, and F. Briones, J. Electron. Mater. **22**(5), 567–572 (1993).
[17]H. Kawanami, A. Hatayama, and Y. Hayashi, J. Electron. Mater. **17**(5) 341–349 (1988).
[18]Y. Li, L. Lazzarini, L. J. Giling, and G. Salviati, J. Appl. Phys. **76**(10), 5748–5753 (1994).
[19]Y. Li, G. Salviati, M. M. G. Bongers, L. Lazzarini, and L. Nasi, J. Cryst. Growth **163**, 195–202 (1996).
[20]S. M. Ting and E. A. Fitzgerald, J. Appl. Phys. **87**, 2618–2628 (2000).
[21]M. Kawabe, T. Ueda, and H. Takasugi, Jpn. J. Appl. Phys., Part 2 **26**(6), L944–L946 (1987).
[22]L. Lazzarini, L. Nasi, G. Salviati, C. Z. Fregonara, Y. Li, L. J. Giling, C. Hardingham, and D. B. Holt, Micron **31**, 217–222 (2000).
[23]M. K. Hudait and S. B. Krupanidhi, J. Appl. Phys. **89**(11), 5972–5979 (2001).
[24]T. Soga, H. Nishikawa, T. Jimbo, and M. Umeno, Jpn. J. Appl. Phys., Part 1 **32**, 4912–4915 (1993).
[25]H. Kroemer, J. Cryst. Growth **81**, 193–204 (1987).
[26]H. Kroemer, J. Vac. Sci. Technol. B **5**, 1150–1154 (1987).
[27]B. Kunert, I. Németh, S. Reinhard, K. Volz, and W. Stolz, Thin Solid Films **517**, 140–143 (2008).
[28]H. Noge, H. Kano, M. Hashimoto, and L. Igarashi, J. Appl. Phys. **64**(4), 2246–2248 (1988).
[29]K. Nauka, G. A. Reid, and Z. Liliental-Weber, Appl. Phys. Lett. **56**(4), 376–378 (1990).
[30]D. B. Holt and B. G. Yacobi, *Extended Defects in Semiconductors: Electronic Properties, Device Effects and Structures* (Cambridge University Press, 2007).
[31]J. Taftø and J. C. H. Spence, J. Appl. Cryst. **15**, 60–64 (1982).
[32]P. Pirouz, C. M. Chorey, and J. A. Powell, Appl. Phys. Lett. **50**(4), 221–223 (1987).
[33]N.-H. Cho and C. B. Carter, J. Mater. Sci. **36**, 4209–4222 (2001).
[34]T. S. Kuan and C.-A. Chang, J. Appl. Phys. **54**(8), 4408–4413 (1983).
[35]D. Cohen and C. B. Carter, Mater. Res. Soc. Symp. Proc. **442**, 503–508 (1996).
[36]J. W. Edington, *Practical Electron Microscopy in Materials Science* (Van Nostrand Reinhold Co., New York, 1976).
[37]K. Morizane, J. Cryst. Growth **38**, 249–254 (1977).
[38]D. R. Rasmussen, N.-H. Cho, D. W. Susnitzky, and C. B. Carter, Ultramicroscopy **30**(1–2), 27–32 (1989).
[39]D. R. Rasmussen, S. McKernan, and C. B. Carter, Phys. Rev. Lett. **66**, 2629–2632 (1991).
[40]N.-H. Cho, S. McKernan, D. K. Wagner, and C. B. Carter, J. Phys. Colloques **49**, C5-245–C5-250 (1988).
[41]V. Narayanan, S. Mahajan, K. J. Bachmann, V. Woods, and N. Dietz, Acta Mater. **50**, 1275–1287 (2002).
[42]F. Ernst and P. Pirouz, J. Mater. Res. **4**(4), 834–842 (1989).
[43]Z. Liliental-Weber, E.R. Weber, L. Parechanian-Allen, and J. Washburn, Ultramicroscopy **26**, 59–64 (1988).
[44]Z. Liliental-Weber, M. A. O'Keefe, and J. Washburn, Ultramicroscopy **30**, 20–26 (1989).
[45]S. H. Huang, G. Balakrishnan, A. Khoshakhlagh, L. R. Dawson, and D. L. Huffaker, Appl. Phys. Lett. **93**, 071102 (2008).
[46]P. D. Nellist, in *Science of Microscopy*, edited by P. H. Hawkes and J. C. H. Spence (Springer, New York, 2007), pp. 65–132.
[47]K. A. Mkhoyan, P. E. Batson, J. Cha, W. J. Schaff, and J. Silcox, Science **312**, 1354 (2006).
[48]E. J. Kirkland, *Advanced Computing in Electron Microscopy* (Plenum, New York, 1998).
[49]M. J. Hÿtch, E. Snoeck, and R. Kilaas, Ultramicroscopy **74**, 131 (1998).
[50]S. Y. Woo, S. Hosseini Vajargah, S. Ghanad-Tavakoli, R. N. Kleiman, and G. A. Botton, J. Appl. Phys. **112**, 074306 (2012).
[51]S. F. Fang, K. Adomi, S. Iyer, H. Morkoç, and H. Zabel, J. Appl. Phys. **68**(7), R31–R58 (1990).
[52]R. D. Bringans, D. K. Biegelsen, and L. E. Swartz, Phys. Rev. B **44**(7), 3054–3063 (1991).
[53]G. A. Devenyi, S. Y. Woo, S. Ghanad-Tavakoli, R. A. Hughes, R. N. Kleiman, G. A. Botton, and J. S. Preston, J. Appl. Phys. **110**, 124316 (2011).

[This article is copyrighted as indicated in the article. Reuse of AIP content is subject to the terms at: http://scitation.aip.org/termsconditions. Downloaded to] IP: 193.62.126.232 On: Wed, 15 Jan 2014 22:01:27